Chapter 4

Self-assembled Bioactive Protein-based amyloidogenic nanohydrogel dressing for rapid diabetic wound healing via enhanced angiogenesis and anti-inflammation

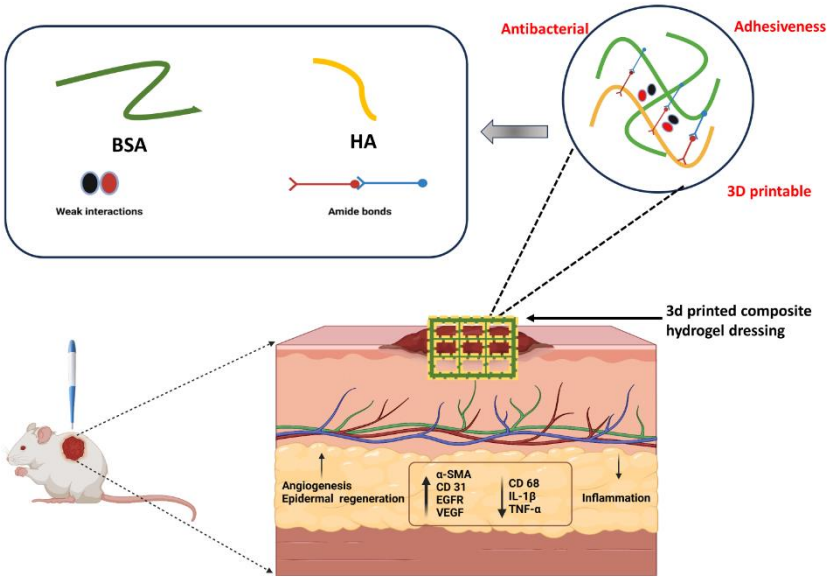

Schematic 2: Schematic illustration of 3D printing of composite BSA-HA hydrogel for rapid diabetic wound healing

4.1 Introduction

As an emerging field, protein nanotechnology offers simple yet powerful design techniques with unique advantages and high potential to develop innovative materials[101],[80], devices[102], and systems[103] at the nanoscale. At the heart of protein nanotechnology is protein engineering, which involves designing and modifying proteins to achieve specific functions[104],[105]. Techniques like directed evolution, site-directed mutagenesis[106], and computational design[107] enable the creation of proteins tailored for applications. This foundational work allows for the development of proteins that act as precise building blocks for nanoscale structures. Another crucial concept is self-assembly, where proteins naturally organize into complex nanostructures through specific interactions[108]. By manipulating these interactions, researchers can construct highly organized materials with nanoscale precision, such as virus capsids[109] and amyloid fibrils[110],[111] repurposed for technological applications. Amyloid fibrils, highly ordered protein aggregates with a characteristic cross-β sheet structure, have garnered significant interest for their potential in nanobiotechnological applications[112]. Traditionally linked to diseases such as Alzheimer's and Parkinson's, these fibrils are now recognized for their exceptional mechanical, structural, and functional properties[113]. Formed through the self-assembly of polypeptide chains into elongated, insoluble fibers, amyloid fibrils exhibit remarkable tensile strength and stiffness, comparable to or exceeding that of silk and other biopolymers[114]. Their robustness and stability make them particularly attractive for creating durable nanomaterials.

In nanobiotechnology, amyloid fibrils-based nanomaterials are being explored for a variety of innovative applications[115],[116]. They can serve as scaffolds for the development of

nanostructured materials, providing a strong and stable framework that can be further functionalized with other molecules[117]. This makes them useful in fabricating advanced composites and coatings with enhanced mechanical properties. Additionally, their biocompatibility, depending on the protein source, opens up possibilities for biomedical applications, such as in tissue engineering and regenerative medicine[118]. Amyloid fibrils can support cell growth and differentiation, providing a structural matrix that mimics natural extracellular environments.

Among them amyloid fibril-based hydrogels are a type of hydrogel that have garnered increasing interest in recent years due to their unique properties and potential applications in biomedicine[119]. These hydrogels are composed of amyloid fibrils, which can self-assemble into highly ordered structures. One of the key advantages of amyloid fibril-based hydrogels is their exceptional mechanical stability and robustness[120]. The fibrillar structure of amyloid fibrils gives them a high degree of mechanical stability, making them ideal for use in hydrogels that must withstand mechanical forces and maintain their shape. Additionally, the high stability of amyloid fibrils makes them resistant to degradation and degradation-induced swelling, which can be a limitation of traditional hydrogels[121]. Another important aspect of amyloid fibril-based hydrogels is their biocompatibility. These hydrogels are composed of proteins, and as such, are biocompatible with cells and tissues. This biocompatibility makes them suitable for a wide range of biomedical applications, including tissue engineering[122] and regenerative medicine[123].

While on other hand, Hyaluronic acid (HA) is a naturally occurring polysaccharide that is found in many tissues throughout the body, including skin, joints, and cartilage. It is effective in promoting wound healing by providing as moist environment for cells to migrate and

proliferate, and by stimulating the production of collagen and other extracellular matrix components[124],[125]. However, there are several limitations such as short residence time, poor mechanical strength, short degradation time, and very high swelling behaviour that need to be considered when using HA hydrogel for wound healing[126].

Taken together, we have developed a 3D printable composite self-assembled amyloidogenic hydrogel comprising BSA protein and HA, which exhibits significantly improved mechanical strength and water retention capacity. In recent years, 3D printing of hydrogels has emerged as a promising approach for advanced wound healing therapies[126]. By precisely controlling the composition and structure, this innovative technique offers tailored solutions for improved wound management and tissue regeneration. Our composite hydrogel demonstrates excellent morphology, in vitro biocompatibility, and suitability for 3D printing, enabling customized dressing formation as described in schematic 2. Moreover, our hydrogel accelerates diabetic wound healing *in vivo* compared to both control and hyaluronic acid alone treated groups. Additionally, we evaluated the efficacy of the hydrogel as a wound dressing material through quantitative and qualitative assessments, including histopathological examination, measurement of collagen content, analysis of gene expressions, and immunohistochemistry studies. Our findings suggest that our customized wound dressing approach, utilizing 3D printing of the hydrogel, holds great potential for translational and clinical applications.

4.2 Results and discussion

4.2.1 Formation of hydrogels

The activation of Hyaluronic acid (HA) by EDC/NHS initiates chemical modifications, as indicated by the emergence of new peaks in specific regions of the ^{1}H NMR spectrum (Fig

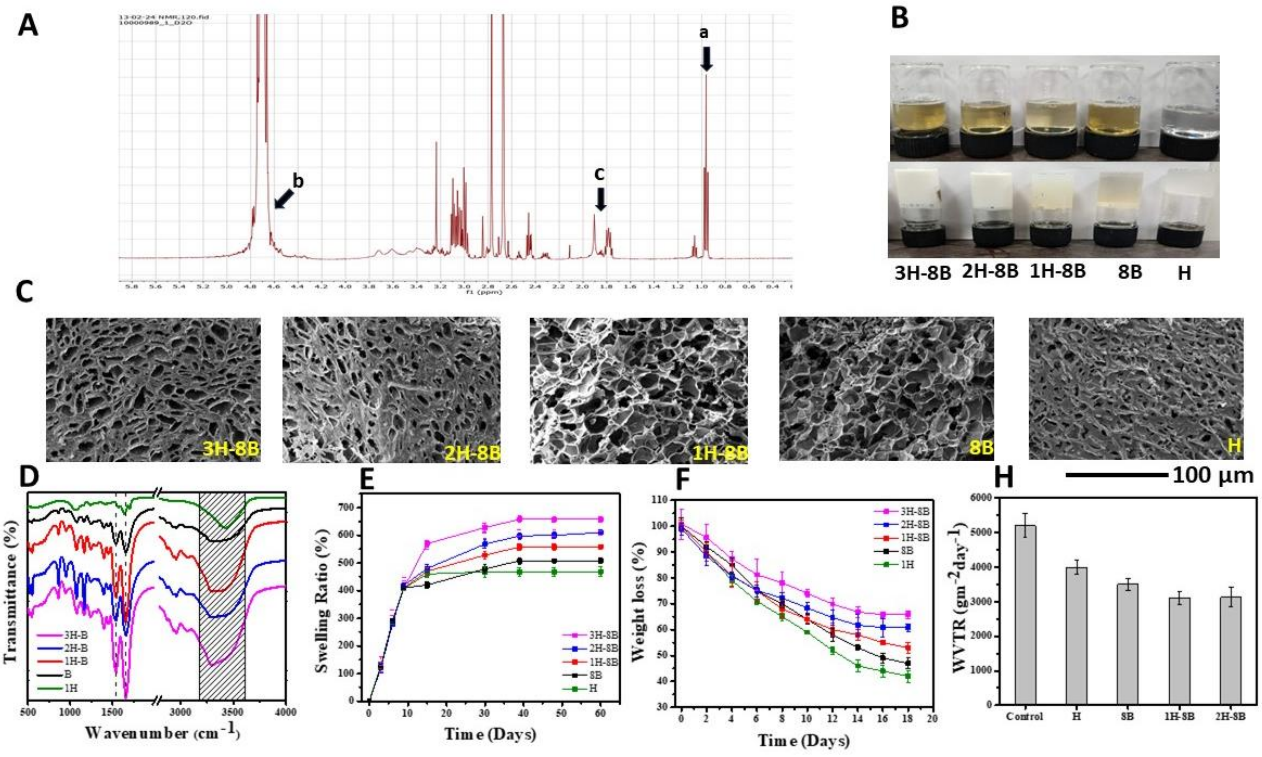

Figure 4.1 Characterizations of hydrogels: (A) 1H NMR spectra of HA activated by EDC/NHS a represents aliphatic group b represents hydroxyl or amino groups and c represents methyl groups (B) Confirmation of formation of hydrogel by vial inversion test: Row 1 represents precursors solution, row 2 represents formation of hydrogel (C) SEM images of hydrogels (D) FTIR spectra: Dashed lines represents Amide I (1520 cm^{-1}) Amide II (1650 cm^{-1}), shaded region represents –OH stretching around 3000-3600 cm^{-1} (E) Swelling ratio (F) Weight loss study and (H) Water vapour transmission rate

4.1A). Peaks between 0.8-1 ppm signify alterations to aliphatic groups, notably methyl protons of aliphatic chains, particularly methylene protons adjacent to the newly formed amide bond. The appearance of peaks at 4.5-5 ppm suggests modifications involving hydroxyl or amino groups, likely due to the formation of amide bonds through EDC/NHS activation[127]. Additionally, peaks at 1.8 ppm indicate changes to methyl or methylene groups within HA or the formation of new groups via coupling reactions[128]. These shifts collectively reveal structural transformations within HA induced by EDC/NHS activation, including the formation of amide bonds and modifications to aliphatic and functional groups.

The BSA-Hyaluronic Acid (HA) composite hydrogel was formed by heating precursor solutions above the melting temperature of BSA. The solution underwent heating until it achieved a translucent gel state, passing the vial inversion test promptly. All preheated solutions exhibited a notably high negative zeta potential, as illustrated in Fig 4.1B. These zeta potential values indicate the presence of elevated surface charges on the protein, ensuring excellent dispersion stability and averting BSA aggregation through electrostatic repulsion. Gel formation was further confirmed using the vial inversion test, as shown in Fig. 1B. Initially, the solution appeared in a liquid state, transitioning into a jiggly gel and ultimately forming a soft gel. Subsequently, the hydrogels underwent lyophilization at -80°C for 24 hours and were stored at 4°C for subsequent analysis. The synthesized hydrogels underwent characterization to explore various physical and chemical properties.

4.2.2 Gelation mechanism

The gelation process of protein-based hydrogel induced by heat near its melting temperature is a well-explored phenomenon, as described in the provided information (mention ref or data

points in figure). The initiation involves BSA aggregation at elevated temperatures and a pH away from its isoelectric point (IEP BSA ~ 4.5). This occurs due to the partial unfolding of BSA molecules, leading to the disruption of hydrogen bonding and the exposure of hydrophobic groups to the solvent. Consequently, the aggregation process is facilitated through intermolecular hydrophobic and electrostatic interactions[127]. Although BSA contains 34 oxidized (disulfide-linked) cysteine residues that could theoretically participate in the aggregation process, the study suggests their absence in the observed gelation, as heating alone cannot break or reduce disulfide bonds[127]. This observation contrasts with prior reports associating the scrambling of disulfide bonds in BSA with amorphous aggregates rather than amyloid fibrils.

Microscopic analysis, specifically through SEM images, revealed formation of an interconnected 3D architecture with micron-sized gaps, crucial for water retention and providing the gel with soft and injectable characteristics. A hypothesis is put forward suggesting that the incomplete β-sheet formation, resulting from retained secondary structures in the proteins, leads to weak intermolecular physical bond formation between denatured proteins. We hypothesize that individual amyloid fibrils, which range in size from several nanometers to tens of nanometers, closely associate with other amyloid fibers to form multimers[68]. These multimers vary in size from five to several tens of microns and collectively create an interconnected three-dimensional structure. This architecture features micron-sized gaps that retain water, giving the gel its soft and injectable properties.

The gelation mechanism of the BSA-Hyaluronic Acid (HA) hydrogel presents a multifaceted process, influenced by the interaction between BSA and HA. The gelation is evidenced by findings from FTIR analysis, indicating an increased intensity of amide bonds in BSA+HA

compared to BSA alone. This observation suggests the formation of new amide bonds, indicative of molecular interactions between BSA and HA. The presence of HA appears to play a significant role in enhancing the gelation process, as supported by rheological studies. Specifically, the storage modulus (G') and loss modulus (G") exhibit an increase with an escalation in the concentration of HA. This rheological behaviour signifies enhanced elasticity and viscosity of the hydrogel with the addition of HA. The observed changes in FTIR spectra, particularly the intensified amide bonds, suggest that the incorporation of HA influences the

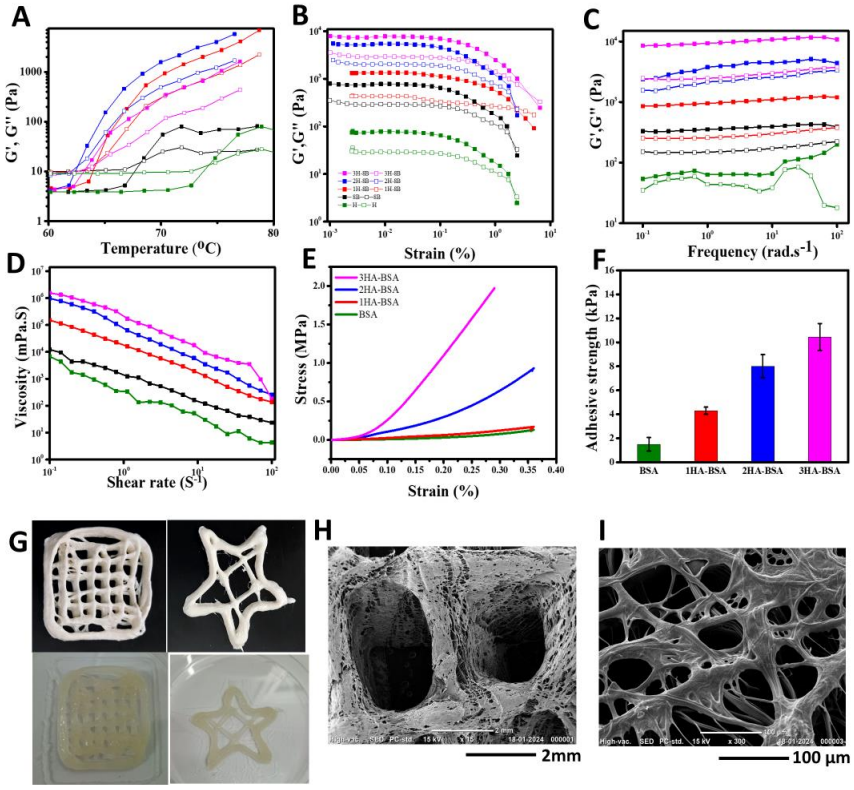

Figure 4.2 (A) Temperature sweep (B) Amplitude sweep (C) Frequency sweep (D) Shear thinning behaviour (E) compression test (F) Adhesion test (G) Fabrication of 3d printed structure using 2H-8B hydrogel row 1 represents lyophilized samples and row 2 represents freshly printed structures SEM images of lyophilized 3d printed (H) mesh structures and (I) Star structure (Scale bar: 2mm)

conformational changes in BSA molecules during the gelation process. The interaction between BSA and HA may involve the formation of new hydrogen bonds or other molecular associations, contributing to the overall gel network. Furthermore, the rheological data indicating an increase in G' and G" with higher concentrations of HA highlight the reinforcing effect of HA on the mechanical properties of the hydrogel. This suggests that the addition of HA not only influences the gelation kinetics but also imparts changes in the viscoelastic properties, potentially leading to a hydrogel with enhanced structural integrity and strength.

In summary, the gelation mechanism of the BSA-Hyaluronic Acid hydrogel is marked by increased amide bond intensity in FTIR, signifying molecular interactions, and heightened G' and G" values in rheological analysis, reflecting improved mechanical properties with increasing HA concentration. These findings underscore the intricate interplay between BSA and HA, offering insights into the gelation dynamics and the potential for tailoring the hydrogel's properties for various biomedical applications.

4.2.3 Characterization of hydrogels

The SEM images of the hydrogels (Fig.4.1C) display a porous structure with visible micron-sized voids. Importantly, the images reveal that increasing HA concentration leads to a reduction in pore size due to enhanced crosslinking (mention respective images). This finding emphasizes the tunability of the hydrogel's structure by adjusting HA concentrations, influencing its physical properties. The morphological analysis also aligns with the understanding that HA forms new amide bonds with BSA within the hydrogel network. This molecular interaction contributes to the stability of the structure, affecting the overall porosity and organization of the hydrogel. Within the SEM images (Fig.4.1C), variations in porosity

are evident among different formulations of the composite hydrogels. For instance, 3H-8B shows an overexpression of HA, leading to a reduction in the degree of porosity in its morphology. On the other hand, 2H-8B emerges as a more advantageous candidate with an optimized and well-organized porosity. This observation underscores the tunability of the hydrogel's structural features by adjusting the concentration of HA.

Fourier-transform infrared (FTIR) spectroscopy revealed characteristic peaks of activated hyaluronic acid (HA) following EDC/NHS treatment (Fig 4.1D). The broad peak at 3500 cm^{-1} confirmed extensive O-H (hydroxyl) stretching, indicating intact disaccharide units and potential hydrogen bonding changes due to activation[127]. Peaks at 1060 cm^{-1} (C-O stretching)[127] and 1640 cm^{-1} (COO^- asymmetric stretching)[127] further corroborated the carbohydrate backbone and retained carboxylate functionality, crucial for bioconjugation. N-H bending (1562 cm^{-1}) and C=O stretching (1705 cm^{-1})[127] of the N-acetyl group highlighted undisturbed disaccharide structure and potential EDC/NHS interaction with primary amine groups. Overall, the FTIR spectrum confirms successful HA activation while preserving its key structural features. Furthermore, in the case of BSA hydrogel, strong and wide peak around 3500 cm^{-1} in the =OH stretching region indicates a lot of hydrogen bonding, suggesting strong compatibility with living cells[129]. Sharp peaks at 1520 and 1650 cm^{-1} show that the protein structure of BSA remains intact in the hydrogel[68]. In the FTIR spectra analysis of the composite BSA-HA hydrogel, no significant changes are observed. There is a discernible increase in intensity in both amide I and amide II bands. This heightened intensity suggests the potential formation of new amide bonds within the hydrogel structure, indicating structural modifications or crosslinking. Interestingly, despite this evidence of bond formation, no distinct emergence of new functional groups is observed. This absence suggests

that the interactions within the composite hydrogel are predominantly weak in nature. The likely contributors to this phenomenon include ionic interactions and hydrogen bonding. The absence of new functional groups implies that the overall chemical composition remains relatively unchanged, supporting the notion of weaker interactions.

The investigation into the lyophilized hydrogel's swelling was conducted to explore its potential for dehydration during transportation/storage and subsequent rehydration for use as a wound dressing. The findings indicated that the composite hydrogels exhibited a notably high swelling ratio, gradually increasing with the concentration of HA over 30 hours, as illustrated in Fig. 4.1E In comparison, the control BSA hydrogel exhibited a 450% swelling ratio after 30 hours. As anticipated, the swelling ratio of the composite hydrogels continued to rise, reaching 550% for 2H-B (A6B8) and 650% for 3H-B. This enhanced swelling ratio in the composite hydrogels is attributed to the hydrophilic properties of HA and BSA, facilitating effective water absorption. The observed high swelling ratio is likely a result of the uniform and interconnected voids within the hydrogels, providing sufficient free volume to accumulate water molecules. The investigation into hydrogel weight loss holds significance for optimizing wound healing. If hydrogel degradation occurs too swiftly, it may fail to provide adequate wound support, impeding the healing process. Conversely, delayed hydrogel degradation might prolong healing, potentially leading to complications like infection. In Fig.4.1F, the weight loss of all examined hydrogels is depicted over a 20-day period. Each hydrogel experienced significant weight loss due to a well-crosslinked polymer network. The decrease in weight loss observed with an increase in hyaluronic acid (HA) concentration in BSA hydrogel may be attributed to the enhanced water-retaining capacity of HA, leading to a more stable and densely crosslinked hydrogel network.

The water vapor transition rate (WVTR) of hydrogels plays a crucial role in their efficacy as wound dressings or biomedical materials. WVTR refers to the rate at which water vapor passes through a material per unit area under specific conditions, typically measured in grams per square meter per day ($g/m^2/day$). The study assessed the water vapor transition rate (WVTR) of various hydrogel formulations. As depicted in Fig.4.1H, the control group exhibited a WVTR of 5200, while hydrogels showed lower rates: 3500 for BSA alone, 3100 for 1HA-BSA, 3132 for 2HA-BSA, and 2832 for 3HA-BSA. This reduction may be attributed to BSA affecting water vapor diffusion, with higher concentrations of hyaluronic acid (HA) resulting in lower WVTR.

4.2.4 Rheological and Mechanical properties

The rheological characterization provides valuable insights into its gelation temperature, shear-thinning behavior, viscoelastic properties, and structural stability. Temperature ramp experiments were conducted to ascertain the gelation temperature and phase changes of the hydrogel compositions. The storage modulus (G') and loss modulus (G'') were plotted against temperature, revealing that the gelation temperature fell between 60 and 75 °C for all hydrogel compositions (Fig.4.2A). The observed inverse correlation between Hyaluronic Acid (HA) concentration, gelation temperature in the BSA-HA hydrogel system suggests a potential mechanism involving the formation of new amide bonds between BSA and HA, as revealed from FTIR spectra. As HA concentration increases, the heightened likelihood of molecular interactions facilitates the formation of amide bonds, contributing to an enhanced cross-linking density within the hydrogel network. This increased cross-linking, driven by amide bond formation, is proposed to reduce the energy barrier for gelation, resulting in a shortened gelation time and lower gelation temperature.

Viscoelastic properties were further assessed through amplitude and frequency sweep tests. The amplitude sweep (Fig 4.2B) revealed the yield stress and linear viscoelastic range (LVR). The hydrogels exhibited a plateau region in G' at a 1% strain, indicative of a consistent, three-dimensional cross-linked network. The addition of HA increased this plateau region, further enhancing the structural stability. The gradual decrease in modulus with an increase in strain explained the injectable and smooth texture of the hydrogels. At low shear rates, the hydrogels displayed predominant elastic behavior (G' > G''), transitioning to dynamic yield stress (G' = G'') and a more viscous nature (G'' > G') at higher shear rates[130].

Additionally, a frequency sweep (Fig 4.2C) in the LVR region demonstrated the predominantly elastic nature of the hydrogels. G' exceeded G" across the frequency range, indicating stability over long-term storage due to a stable network of forces. Both G' and G'' remained nearly constant and independent across the frequency range from 0.1 to 10 rad s^{-1}, emphasizing the structural stability and elastic nature of the hydrogel[75].

The rheological properties crucial for 3D extrusion were evaluated, emphasizing the necessity of shear-thinning behavior in hydrogels for extrusion-based 3D printing. The hydrogels exhibited excellent shear-thinning behavior (Fig. 4.2D), indicating the formation of uniformly cross-linked structures. Under shear, the hydrogels demonstrated the breakdown of superstructures into aggregates, forming an immobilized hydrogel network capable of moving with increasing shear rate[14]. Remarkably, all hydrogels displayed similar shear-thinning behavior across a range of shear rates.

Evaluation of essential mechanical properties, such as stability and elasticity crucial for wound dressing hydrogels, was conducted through a compression test. As illustrated in Fig.

4.2E, all composite hydrogels exhibited outstanding stability, maintaining structural integrity during the compression test. Furthermore, these hydrogels displayed soft and stretchable behavior, indicative of a high degree of crosslinking facilitated by the substantial water content in the hydrogel pores. The addition of hyaluronic acid (HA) significantly altered the compression modulus, particularly at higher concentrations, suggesting the formation of a robust matrix strengthened by numerous hydrogen bonds with HA. In summary, the composite hydrogels demonstrated a compression modulus that aligns with the requirements for wound healing and tissue engineering applications, showcasing compatibility and consistency with reported findings.

The intermolecular interactions between HA and BSA could further contribute to the structural integrity, mitigating degradation. In the initial phase of wound healing, the effective adhesion of the hydrogel plays a crucial role[131]. By forming a strong bond, the hydrogel acts as a physical barrier that adheres to the wound, preventing the outflow of blood and facilitating physical haemostasis[132]. Hence, the adhesive characteristics of composite hydrogels underwent examination through lap shear strength experiments. The hydrogel was applied on porcine tissue and allowed to set at 37°C for 4 hours . The adhesive strength of the composite hydrogels exhibited an increment, rising from the initial 7.3 ± 0.3 kPa to 13.4 ± 1.13 kPa as the concentration of HA increased (Fig. 4.2F). This observed enhancement in adhesion is attributed to the formation of ionic and hydrogen bonds between the hydrogel and the substrate.

4.2.5 3D printing of hydrogel

Achieving optimal outcomes in the 3D printing of hydrogels hinges on thorough considerations of shape fidelity and integrity[58]. The extrusion method, as observed, holds distinct advantages for bioprinting, offering versatility, high-throughput capabilities, controlled resolution, and accessibility. In Fig. 4.2G, successful printing of a mesh and star structures using the 2H-B hydrogel shows its potential for high shape fidelity[133]. The 2H-B hydrogel's exceptional porous morphology and high swelling ratio contribute to its ease of flow under printing conditions, with subsequent thickening after extrusion, facilitated by a lower yield stress than the stress applied to the nozzle tip. These properties ensure accurate and resolution-focused printing using a 22 G needle. Concerns about distortion or collapse during or after printing are addressed by the 2H-B hydrogel's self-supporting nature, as each layer remains intact throughout the process. The SEM image in Fig. 4.2(H, I) showcases the structural integrity and high porosity of the freeze-dried 2H-B hydrogel sample. This porous characteristic is highly advantageous for specific applications like tissue engineering and drug wound healing, allowing the exchange of nutrients and other substances between the hydrogel and its surroundings. These results highlight the potential of our composite hydrogel for successful 3D printing, ensuring good shape fidelity and integrity. Additionally, its unique properties, such as self-supporting and shear-thinning behaviour, position it as a promising candidate for a broad range of 3D printing applications.

4.2.6 Antibacterial studies

To evaluate the antibacterial properties of the composite hydrogel, an ideal wound dressing should exhibit the ability to protect against external bacteria, restrict the spread of

microorganisms at the wound site, and alleviate inflammation[134]. In this study, *S. aureus* and *E. coli* were employed to assess the surface antibacterial efficacy of the hydrogels (Fig

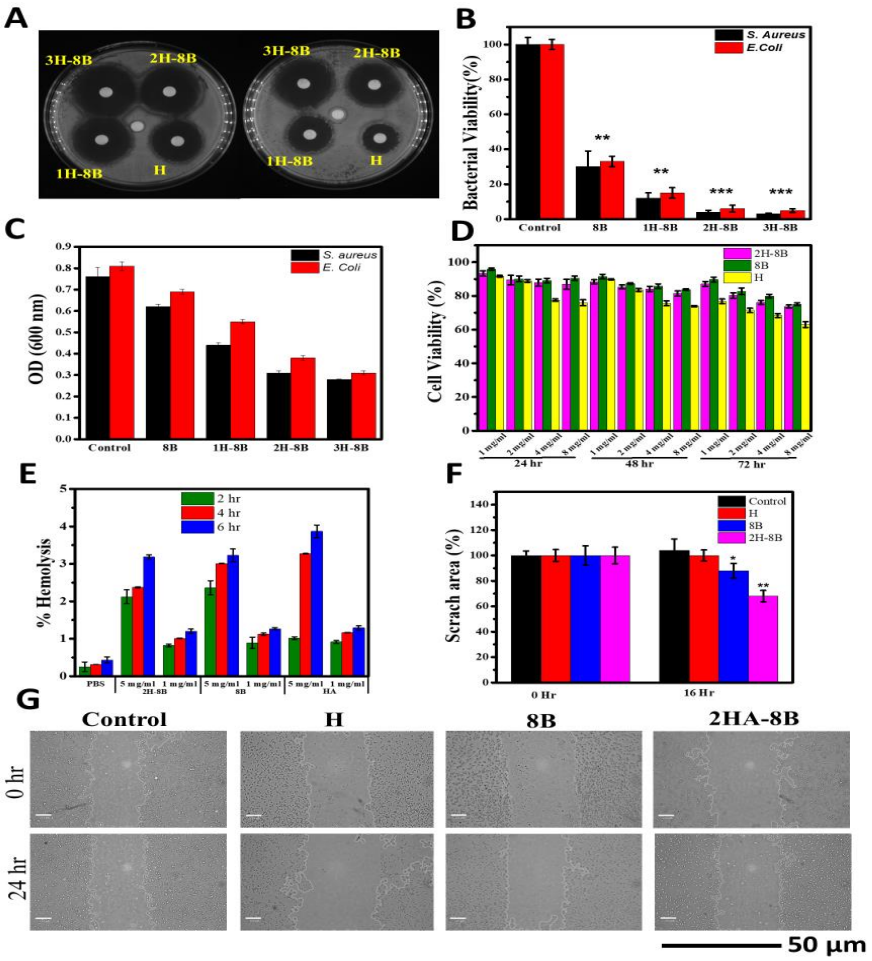

Figure 4.3 (A) Agar plate images of inhibition of S.aureus and E.coli with treatment of hydrogels (B) Percentage bacterial viability of S.aureus and E.coli when treated with hydrogel (C) Optical density at 600 nm in turbidity test (D) Cell viability profile of NIH-3T3 on hydrogels after incubated for 24 hr, 48 hr and 72 hr (E) Ex vivo hemolysis of hydrogels with RBCs after 2 hr, 4 hr and 6 hr (F) Extent of wound closure in sctrach assay after o hr, 16 hr and 32 hr (G) Time lapse images of wound healing closure of NIH-3T3 cell treated with hydrogels over 0 hr, 16 hr and 32 hr, Scale bar: 50 µm (* $P < 0.05$, ** $P < 0.01$, *** $P < 0.001$)

4.3A). Following a 24-hour incubation period at 37°C, the 2H-8B hydrogels demonstrated a bacterial cell killing rate exceeding 80% for both *S. aureus* and *E. coli* (Fig 4.3B), indicating their effectiveness in impeding bacterial growth. The observed inhibition zone signifies a reduction in the bacterial colony population in that specific region. The outcome illustrated in Fig. 4.3C indicates a significant rise in the OD600 value of the control group, lacking antibacterial agents, after 24 hours of culturing Furthermore, the results indicate a concurrent increase in antibacterial activity with elevated concentrations of HA. Therefore, we deduce that all composite hydrogels exhibit antibacterial activity. The antimicrobial activity of the hydrogel formed by self-assembling bovine serum albumin (BSA) and hyaluronic acid (HA) can be attributed to HA. Hyaluronic acid (HA) plays an active role in inhibiting microbial growth. HA can interact with the bacterial surface and impede the microbial adhesion process. Since bacterial colonization often starts with surface adhesion, HA helps prevent the formation of biofilms, making it harder for bacteria to grow and proliferate.

4.2.7 *In vitro* studies

Biocompatibility assessment is imperative for the development of biomedical compounds. In this study, hydrogel biocompatibility was tested via the MTT colorimetric method to gauge cell viability percentages. This technique involves the conversion of MTT to purple formazan crystals by mitochondrial dehydrogenase in viable cells. NIH-3T3 cells were exposed to various concentrations of hydrogels (1-8 mg/ml) for 24, 48, and 72 hours, and subsequent cell viability was assessed. A dose- and time-dependent decline in cell viability was noted for all hydrogels, particularly evident in HA hydrogel, where viability dropped by approximately 25-30% after 72 hours. Nevertheless, none of the composite hydrogel concentrations exhibited toxicity to NIH-3T3 fibroblast cells, with cell viability remaining at around 74-77%

even at the highest concentration of 8 mg/ml after 72 hours. Minor variations in cell viability were attributed to synthesis agent concentrations. The data, illustrated in Fig. 4.3D, suggest that the prepared hydrogels did not impede fibroblast cell mitochondrial metabolism, thus indicating promise for biomedical applications such as drug delivery and wound healing. Furthermore, a hemolysis assay was conducted to further assess hydrogel biocompatibility (Fig. 4.3E). This assay serves as a straightforward and reliable means of evaluating material biocompatibility. Results indicated minimal hemolytic activity for hydrogels at concentrations of 1 mg/ml and 5 mg/ml compared to the positive control across 2, 4, and 8 hours. Interactions with red blood cells demonstrated hemolysis percentages below 5%, meeting the critical safe hemolytic ratio for biomaterials as per ISO/TR 7406, signifying minimal damage to RBCs even after 8 hours of incubation at the study's concentrations. In conclusion, the findings affirm the biocompatibility of the investigated hydrogels, positioning them as potential candidates for biomedical applications. Both the MTT assay and hemolysis assay revealed no significant cytotoxicity to cells or RBCs, respectively, suggesting the viability of conducting further *in vivo* studies to explore their efficacy in biomedical contexts.

Additionally, the effect of hydrogel-containing medium on wound healing was investigated using an *in vitro* cell model. Results (depicted in Fig. 4.3F, G) demonstrated the hydrogel's promotion of wound healing, evidenced by reduced scratch area and width after 24 hours of exposure compared to the control group. Notably, the rate of cell migration increased after hydrogel exposure, averaging 5.21 μm/hr from 24 hours until the end of the experiment, suggesting potential applications in enhancing wound healing.

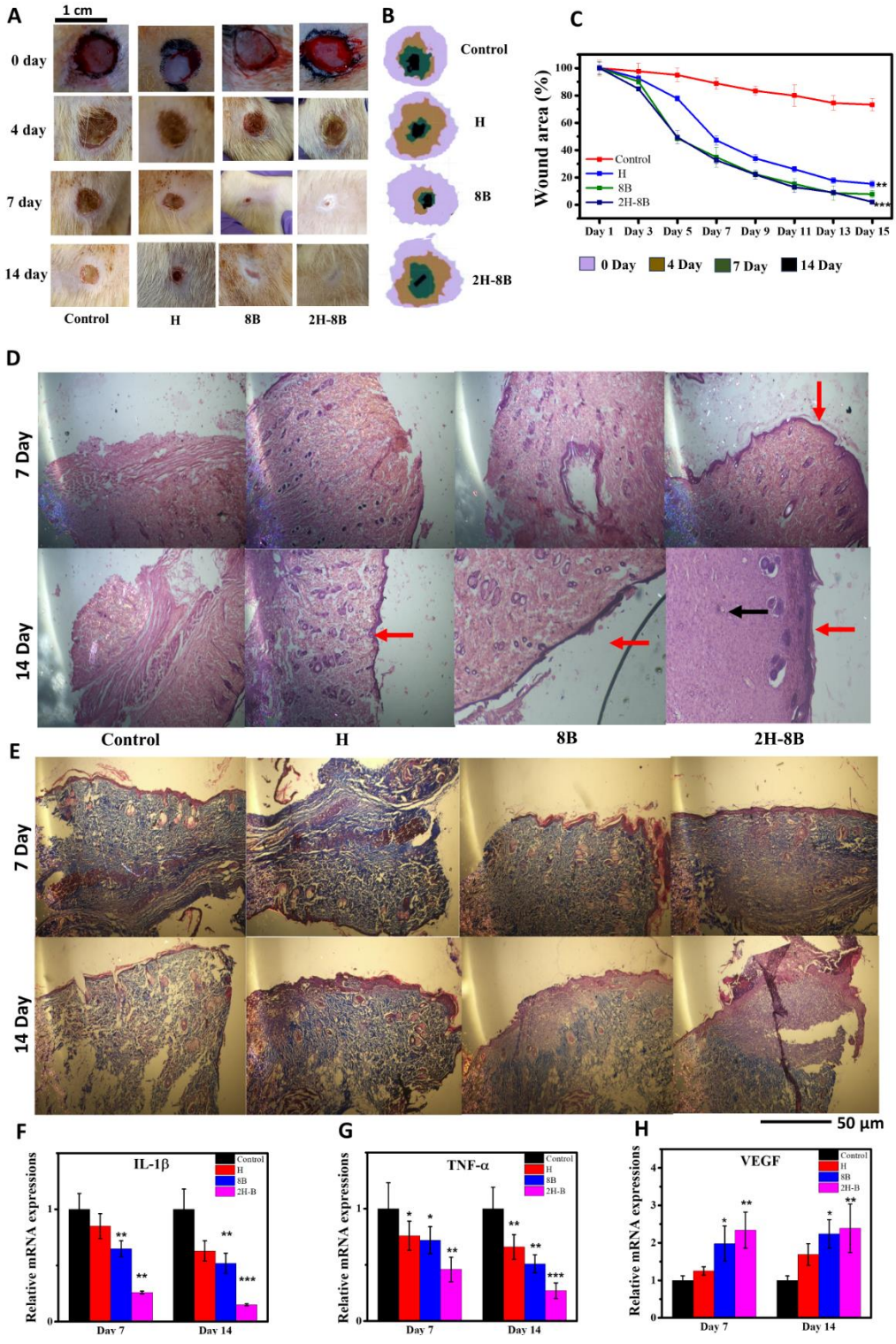

Figure 4 (A) Pictorial representation of assessment in vivo wound healing on days 0, 4, 7 and 14 (B) Traces of wound closure on days 0, 4, 7 and 14 (C) Wound area closure rate of control

and treated groups post wound formation (D) H&E staining of control, H 8B and 2H-8B treated group on days 7 and 14 red arrow represents formation of granulation tissue while black arrow represents formation of epidermis layer (E) Masson staining of control, H 8B and 2H-8B treated group on days 7 and 14, (Scale bar: 50 μm) Gene expressions of (F) VEGF (G) IL-1β and (H) TNF-α analysed by qRT-PCR on days 7 and 14 (* $P < 0.05$, ** $P < 0.01$, *** $P < 0.001$)

4.2.8 *In vivo* studies

Delayed wound healing is a common issue in individuals with Diabetes mellitus, attributed to the persistent hyperglycemic condition[135]. Utilizing the beneficial wound healing properties of HA represents a strategic approach for addressing this challenge in diabetic conditions. Our study focuses on enhancing wound healing through the topical application of hydrogels via 3d printed customized dressing, an innovative alternative to conventional methods. In this *in-vivo* study, hydrogels derived from BSA, HA, and a composite of BSA and HA were evaluated for their potential to promote healing in a chronic diabetic wound model induced in Wistar rats using streptozotocin (STZ). STZ, a diabetogenic agent with alkylating antineoplastic properties, is widely employed to induce diabetes mellitus for assessing hydrogel healing properties[136]. The administration of STZ results in damage to insulin-producing beta cells of the pancreas, characterized by DNA fragmentation and apoptosis[136]. Reactive oxygen species, including hydrogen peroxide, accumulate, exacerbating cellular dysfunction, leading to impaired insulin production and hyperglycemia. Diabetes was induced in the rat model with a dose of STZ ranging from 50 to 65 mg/kg. Validation of the diabetes mellitus model was confirmed by measuring glucose levels, with

levels exceeding >250mg/dL indicating induced diabetes[136]. Subsequently, excisional wounds were formed for diabetes-related studies. Throughout the experiment, macroscopic qualitative analysis revealed differences in wound area and morphology among the groups as depicted in fig 4.4(A, B). Scar formation, inflammation signs, and re-epithelialization were observed, with the 2H-B treated group showing a faster re-epithelialization rate. Wound area and closure rate analysis (Fig. 4.4C) indicated that the diabetic wound+2H-B treated group exhibited more rapid contraction compared to the control (73.24±4.59%) and For the HA treated and BSA treated groups, the values were 15.26±2.53% and 7.80±2.76%, respectively. These findings suggest enhanced healing with a combination of both BSA and HA in comparison to the diabetic wound control.

The quality of regenerated skin was assessed using histological techniques including hematoxylin and eosin (H&E) staining (Fig 4.4D) and Masson's trichrome staining (Fig 4.4E). In the control group, evident inflammatory infiltration characterized by the presence of macrophages and lymphocytes was observed, indicating a pronounced inflammatory response in the area[137]. In contrast, the hydrogel-treated groups exhibited a higher density of well-organized fibroblasts and the emergence of neovascularization indicated by red arrow. Notably, the 2H-8B group displayed a fully integrated new epidermis tightly adhered to the underlying granulation tissue, whereas other groups showed a looser connection. Furthermore, wound healing progressed to the remodelling stage in the 2H-8B group, leading to increased thickness of granulation tissue and epidermis indicated by red and black arrows respectively. Collagen deposition and arrangement are critical indicators of wound healing quality due to their role in subcutaneous connective tissue integrity[138]. Masson's trichrome staining revealed that the control group exhibited accumulation of muscle fibres and cellulose

with relatively low interstitial collagen content. In contrast, the 2H-8B hydrogel-treated wounds displayed the highest and most uniformly distributed collagen fibres among all groups, indicative of improved extracellular matrix (ECM) and tissue remodelling. These findings suggest that the 2H-8B hydrogel promotes collagen deposition and corrects the aberrant state of deposited collagen fibres, thereby facilitating diabetic wound healing.

4.2.9 Real-Time qRT-PCR analysis

To confirm the expression of inflammatory and proangiogenic factors at the gene level, RT-qPCR was employed to assess mRNA levels at 7- and 14-days post-treatment. In the early stages of diabetic wound healing, upregulation of pro-inflammatory cytokines such as IL-1β and TNF-α occurs as part of the acute inflammatory response, which is essential for the wound healing process[139],[140]. However, excessive expression of these cytokines can impede healing progress. The RT-qPCR data revealed that untreated wounds exhibited higher levels of IL-1β (Fig. 4.4F) and TNF-α (Fig 4.4G) gene expressions compared to wounds treated with H, 8B, and 2H-B, where expression levels gradually decreased. During the proliferative phase, VEGF is upregulated, while it is downregulated during the remodelling stage[141]. The mRNA concentrations of VEGF (Fig. 4.4H) in tissues from wounds treated with 2H-8B and H were 2.5 and 2.0 times higher, respectively, than those in untreated wounds at both 7 and 14 days. Furthermore, VEGF expression in 2H-8B treated wounds peaked at 7 days and remained stable thereafter, suggesting that 2H-8B hydrogel promotes wound repair while preventing excessive collagen deposition and scar formation. These findings indicate that the combination of BSA and HA, specifically 2H-8B hydrogel, enhances VEGF expression and promotes neovascularization in the treated wound area. While further investigation into the mechanism of action of HA is warranted, it can be hypothesized that the synergistic effects

of its antimicrobial and anti-inflammatory properties contribute to enhancing the wound healing process.

4.2.10 Immunohistochemical staining analysis

We performed IHC staining for α-SMA (Fig. 4.5A), CD31(Fig. 4.5B), CD68(Fig. 4.5C), EGFR (Fig. 4.5D), and β-catenin (Fig. 4.5E) at the wound sites to understand the molecular mechanisms of hydrogel-mediated wound healing**.** In diabetic wounds, impaired myofibroblast function can hinder healing processes, leading to chronic wounds[136]. Monitoring alpha-SMA expression provides valuable insights into the activation and function of myofibroblasts[136]. The increase in α-SMA expression (Fig. 4.5F) in the 2H-B group indicates improved functional neovascularization, which is essential for the establishment of a robust vascular network within the wound. This finding suggests that the 2H-B hydrogel may enhance the recruitment and differentiation of perivascular cells, promoting the maturation and stability of newly formed blood vessels.

The expression of CD31 is crucial because it indicates the formation of new blood vessels, a process known as angiogenesis[136]. In the context of wound healing, angiogenesis is essential for supplying oxygen and nutrients to the wound site, facilitating tissue repair and regeneration. The observation of increased CD31 expression (Fig. 4.5G) in the 2H-B group suggests that this hydrogel formulation promotes angiogenesis more effectively compared to the other groups. This finding is particularly significant in diabetic wound healing, where impaired angiogenesis can severely compromise the healing process[136]. In parallel, CD68 is a marker for macrophages, which play a vital role in the inflammatory phase of wound healing[136]. The decrease in CD68 expression (Fig. 4.5H) over time in the 2H-B group indicates a more efficient resolution of inflammation, which is essential for transitioning to

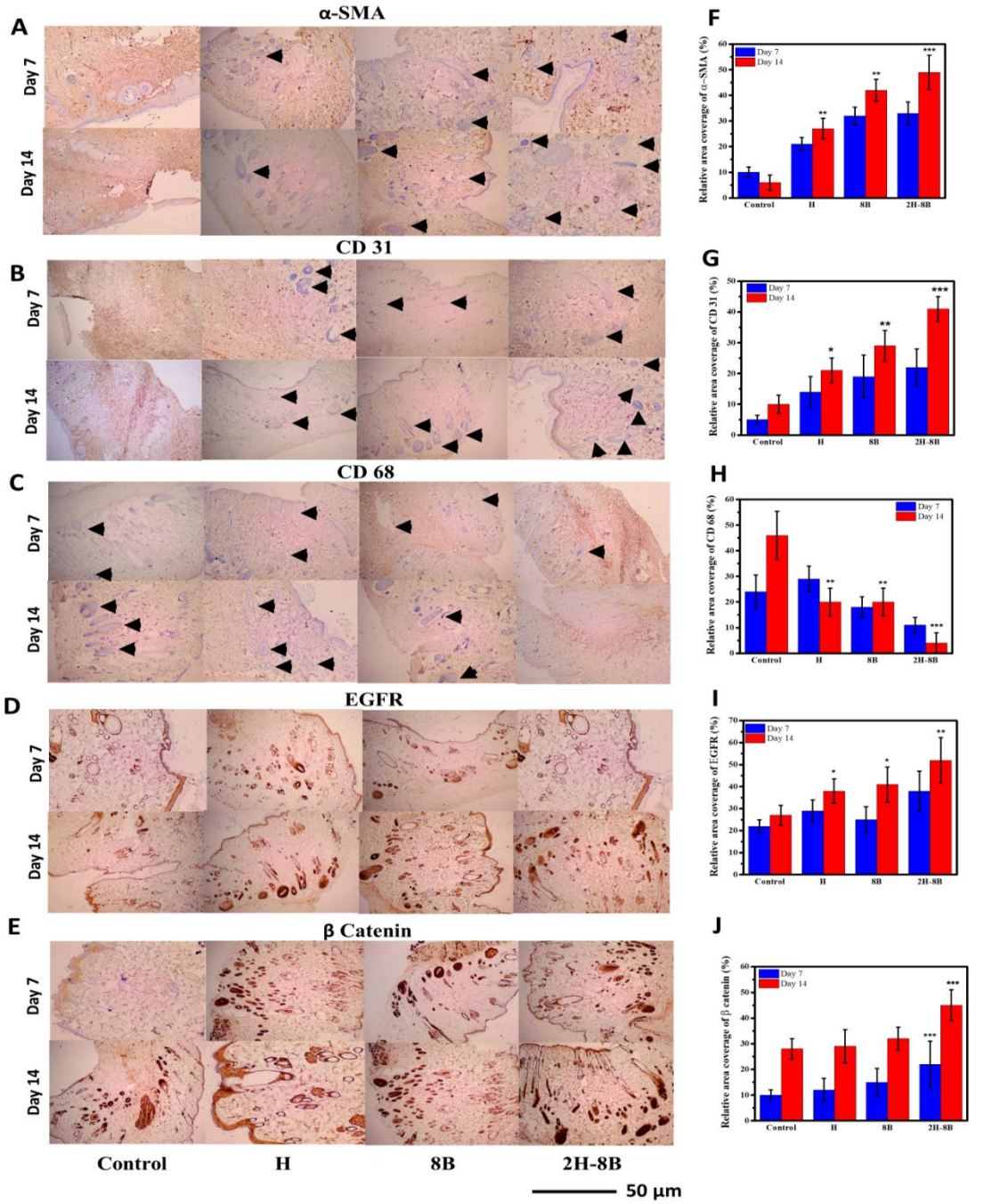

Figure 4.5 Immunohistochemical staining analysis of skin wounds post wound formation on day 7 and 14 with (A-E) α-SMA, CD 31, CD 68, EGFR and β Catenin (Scale bar: 50 µm), Quantitative analysis of (F) α-SMA, (G) CD 31, (H) CD 68, (I) EGFR and (J) β Catenin

the proliferative phase of wound healing[136]. The lower expression of CD68 in the 2H-B

group compared to the control group suggests that this hydrogel formulation may help modulate the inflammatory response, leading to faster and more efficient wound healing. Moreover, the expression of EGFR is associated with the enhancement and maturation of epidermal tissues[142]. The significant expression of EGFR (Fig. 4.5I) in the 2H-B group on day 7 implies accelerated epidermal regeneration, which is crucial for wound closure and the formation of new skin tissue. This finding suggests that the 2H-B hydrogel may stimulate the proliferation and migration of epidermal cells, contributing to faster wound closure and improved tissue repair. Also, the expression of β-catenin (Fig. 4.5J) is associated with the regulation of cell proliferation and the initiation of the healing process[141]. The significant expression of β-catenin in all treated groups suggests that the hydrogel formulations may promote cell proliferation and tissue regeneration. However, the regular pattern of β-catenin expression observed in the 2H-B group suggests a more coordinated and efficient healing process, potentially leading to enhanced tissue regeneration and wound closure.

Overall, the findings of the study suggest that the 2HA-B hydrogel-based dressing patch exerts multiple beneficial effects on the wound healing process. By promoting angiogenesis, modulating inflammation, stimulating epidermal regeneration, enhancing neovascularization, and regulating cell proliferation, this hydrogel formulation accelerates wound healing and improves tissue repair compared to conventional HA hydrogel formulations.

4.3 Conclusion

In summary, our research has successfully developed a 3D printed dressing using a composite nanohydrogel consisting of bovine serum albumin (BSA) protein based amyloid fibrils and hyaluronic acid (HA) employing a one-step process. This hydrogel formulation exhibits

impressive characteristics, including exceptional water holding capacity, rheological properties, advantageous morphological features and crucially, 3D printability. *In vitro* investigations have revealed the outstanding biocompatibility of all hydrogel variants with both NIH 3T3 cells and blood cells. Particularly enhanced performance of the 2H-8B hydrogel, which demonstrates superior cell migration and proliferation compared to individual hydrogel (8B and H) components in scratch assay. *In vivo* studies have showcased the remarkable efficacy of the 2H-8B dressing in fostering an optimal moist environment conducive to the expedited healing of diabetic wounds. This accelerated healing process significantly outperforms other treatment groups. Additionally, our findings highlight the multifaceted therapeutic potential of the 2H-B hydrogel, which not only promotes crucial processes such as angiogenesis and epidermal regeneration but also facilitates substantial collagen deposition and neovascularization. Moreover, the anti-inflammatory and immunosuppressive properties inherent in HA contribute to a notable reduction in inflammation associated with wound healing. In conclusion, the 2HA-8B hydrogel represents advancement with substantial implications for the development of various wound healing modalities. Beyond its application in 3D printed dressings, this innovative hydrogel formulation holds significant promise for the design of biodegradable sutures and patches, offering convenient and effective solutions for diabetic wound management.